

Statistical properties of the Bipolar Magnetic Regions

Dong Li¹

Key Laboratory of Dark Matter and Space Science, Purple Mountain Observatory, Chinese Academy of Sciences, Nanjing 210008, China; lidong@pmo.ac.cn

Abstract Using the observations from Michelson Doppler Imager (MDI) onboard Solar and Heliospheric Observatory (SOHO), we develop a computational algorithm to automatically identify the bipolar magnetic regions (BMRs) in the active regions, and then study their statistical properties. The individual magnetic (positive or negative) pole of the BMR is determined from the region with an absolute strength above 55 G and with an area above 250 pixel² (~ 495 Mm²), while a BMR is identified as a pair of positive and negative poles with a shortest area-weight distance between them. Based on this method, 2234 BMRs are identified from the MDI synoptic magnetograms between the Carrington Rotation 1909 (1996 May 06) and 2104 (2010 December 10). 1005 of them are located in the northern hemisphere, while the other 1229 are in the southern hemisphere. We find that the BMR parameters (e.g., latitudes, separations, fragments, and strength) are similar to those of active regions (ARs). Moreover, based on the maximum likelihood estimation (MLE) method, the frequency distributions of these BMRs occurrence as functions of area size and magnetic flux exhibit a power-law behavior, i.e., $dN/dx \propto x^{-\alpha_x}$, with an index of $\alpha_A = 1.98 \pm 0.06$ and $\alpha_F = 1.93 \pm 0.05$. We also find that their orientation angles (θ) follow the “Hale’s Polarity Laws” and deviate slightly to the solar equator direction. Consistent with the previous findings, we obtain the orientation angles dependence on the latitudes for the normal BMRs during the 23rd solar cycle. The north-south asymmetry of these BMRs is also detected here.

Key words: methods: statistical; Sun: activity; Sun: magnetic fields

1 INTRODUCTION

The magnetic fields are believed as the dominant reasons for the evolution of solar activity, while the stronger and larger magnetic fields on the solar surface are mainly in the active regions (ARs). Meanwhile, most of the energetic and geo-effective events take place at the ARs, such as solar flares, coronal mass ejections (CMEs), solar energetic particle events, and eruptive prominences. Therefore, quantitative study the magnetic fields in the ARs is important to the basic solar physics. As earlier as more than 350 years ago, ARs have been studied as sunspots on white light images (e.g., Wolf, 1861; Maunder, 1904; McKinnon & Waldmeier, 1987; Hathaway et al., 1999; Li et al., 2001; Hathaway et al., 2003; Zhang et al., 2010; Jiang et al., 2011; Hathaway, 2010). It is well known that the number of the sunspots on solar disk display a periodic behavior, which has an average period of about 11 years. And the positions of the sunspots exhibit the butterfly shapes, which is well-known as “Butterfly Diagram”, this suggests that the behavior of the sunspot follows the “Spörer’s Law of Zones”. The sunspots are those regions with stronger magnetic fields on the Sun, and their magnetic nature is followed by the famous “Hale’s Polarity Laws”. Both the unipolar spots and the preceding members of the bipolar spots, their magnetic polarity is negative before the last sunspot minimum and positive since the solar minimum in the northern hemisphere, while in the southern hemisphere, their magnetic polarity is positive

before the last sunspot minimum and negative since the solar minimum (Hale et al., 1919). That is to say, the signs of the sunspot could be reversed at the solar minimum, thus the period of the solar magnetic fields is about 22 years, which is called as solar magnetic cycle.

The characteristics of the magnetic fields at ARs have been reported by many authors (e.g., Howard, 1989; Wang & Sheeley, 1989; Harvey & Zwaan, 1993; Zhang et al., 2010). Using the Mount Wilson daily magnetogram data set, Howard (1989) presented various properties of the magnetic fields at solar ARs. For example, the average separation of the magnetic polarity was about 7 deg (~ 86 Mm), the distribution of the magnetic flux per AR showed a peak of about 2×10^{21} Mx. This was similar to the value of 4×10^{21} Mx obtained by Wang & Sheeley (1989), who used the data from National Solar Observatory/Kitt Peak during 1976–1986. Latter, Harvey & Zwaan (1993) studied the properties of the ARs from the NSO/KP full-disk magnetogram during 1975–1986 throughout Solar Cycle 21, and their conclusion was that the shape of the characteristic size distribution for the ARs was a fundamental invariant property of solar magnetic activity. Recently, using the high-resolution synoptic magnetograms constructed from SOHO/MDI image during 1996–2008, Zhang et al. (2010) identified 1730 ARs and quantified their physical properties. The mean and maximum magnetic flux of the individual ARs were 1.67×10^{22} Mx and 1.97×10^{23} Mx, while those of each Carrington rotation were 1.83×10^{23} Mx and 6.96×10^{23} Mx, respectively.

A number of literatures (e.g., Bogdan et al., 1988; Abramenko & Longcope, 2005; Canfield & Russell, 2007; Zhang et al., 2010) have reported the distribution of magnetic flux or area of ARs and sunspots. These papers reported that the distribution related to ARs are usually log-normal. For example, Zhang et al. (2010) have analyzed the frequency distribution of ARs, and found that the distribution with the function of area size and magnetic flux following a log-normal function, this was consistent with the results obtained by Abramenko & Longcope (2005) and Canfield & Russell (2007). And Bogdan et al. (1988) found the sunspot umbral area were distributed lognormally with Mount Wilson white-light data in the interval between 1917 and 1982. However, Parnell et al. (2009) analyzed the magnetograms from SOHO/MDI and Hinode/SOT, they found that all feature fluxes following the power law distribution with a slope of 1.85 ± 0.14 . While Tang et al. (1984) studied the 15 years of ARs data using the Mount Wilson daily magnetograms data from 1967 to 1981, and their results revealed that the number of the ARs decreased exponentially with the increasing AR sizes. This was also proved by Zharkov et al. (2005), who found that the number of sunspots growing nearly exponentially with their area decreasing. Meanwhile, Harvey & Zwaan (1993) have successfully used the polynomial function to fit the NSO/KP data. These different fit functions are caused by the different observation data, and they may be related to the physical mechanism of the ARs emergences. The log-normal distribution has been regarded as the result of magnetic fragmentation in the solar envelope (Bogdan et al., 1988). While the log-normal distribution of the AR's flux may also suggest that the process of fragmentation dominates over the process of concentration in the formation of the magnetic structure in ARs (Abramenko & Longcope, 2005; Canfield & Russell, 2007). On the other hand, the power-law distribution of the AR's flux possibly suggests a self-similar nature of all ARs (McAteer et al., 2005). If considering the magnetic flux between 2×10^{17} Mx and 10^{23} Mx, then the power-law distribution also suggests that the mechanisms of the surface magnetic features are scale-free (Parnell et al., 2009). Finally, Schrijver et al. (1997) thought that the exponential distribution was lead by the frequent fragmentation and collision (or merging) of the magnetic features.

The orientation angles of the magnetic fields at ARs are important to understand the solar physics, they not only represent the important quantity that is related to the large-scale properties of magnetic field distribution, but may be also related to the dynamo progress which is believed to lead the solar activity cycle (Babcock, 1961; Leighton, 1964, 1969; Sheeley et al., 1985). Howard (1989) have studied the orientation angles of the magnetic regions at ARs with Mount Wilson magnetograms. He found that the distribution of ARs orientation angles showing two broad maxima centered on the 'normal' orientation, and the reversed oriented ARs tending to be relatively evenly distributed in orientation angle compared to the normally oriented ones. However, the most studies are the tilt angles of the magnetic regions, which are similar to the orientation angles but not the same. The orientation angle is defined as the angle from the positive/negative towards negative/positive fields (Howard, 1989). While the tilt angle is

defined to be the angle between the bipolar axis line and heliographic east-west line (Wang & Sheeley, 1989), it is the angle measured positive for magnetic regions with leading fields equatorward of following fields and negative for magnetic regions with leading fields poleward of following fields (Howard, 1991a; Li & Ulrich, 2012). In other word, the tilt angle is very useful to study the Hale's and Joy's laws (Li & Ulrich, 2012), while the orientation angle only exhibits the incline of the ARs on solar disk. The first detailed study the tilt angles of the magnetic regions is Hale et al. (1919), who found that the average tilt angles of sunspots increasing with solar latitudes. This result was confirmed by Brunner (1930), who also found that the larger, well-developed sunspots tending to have small tilt angles than the smaller, less-developed ones. Then Wang & Sheeley (1989) used the NSO magnetograms to find that the average tilt angles of all BMRs relating to the east-west line showed a progressive increasing toward high latitude, and the value was close to 9° . After that, Howard (1991a) studied the tilt angles of the magnetic regions in ARs with Mount Wilson magnetograms, he found that the variation of tilt angles with solar latitudes was not dependent on the solar cycle phases. These ARs with the larger absolute tilt angles have the rapid separation of the magnetic poles on average, and their sizes are smaller than those with smaller absolute tilt angles. Lately, Howard (1991b) studied the tilt angles of the sunspots with Mount Wilson daily white-light photographs, he obtained the similar results to the earlier studies about ARs (e.g., Wang & Sheeley, 1989; Howard, 1991a), and the average tilt angle of the sunspots was 4.2 ± 0.2 degree in his study.

In this paper, we automatically identify the BMRs in the ARs with the high-resolution Carrington rotation synoptic magnetogram charts constructed from SOHO/MDI observations between 1996 and 2010, and then study their orientation angles. This paper is organized as following: the observation and data reduction are introduced in Section 2, and the observation results are given in Section 3, then our conclusions and discussions are given in Section 4.

2 OBSERVATIONS AND DATA REDUCTION

2.1 Observations

The data used here are from the SOHO/MDI magnetograms (Scherrer et al., 1995). MDI is designed to measure the velocity, intensity and magnetic fields in the photosphere, and further to study the magnetic fields in the corona. It can be detected the full solar disk magnetogram with the spatial resolution of $\sim 2'' \text{ pixel}^{-1}$ in every 96 minutes (Domingo et al., 1995). However, the full disk MDI magnetograms are not used directly in this paper, but the Carrington Rotation (CR) synoptic charts are used to analyze, and they can be downloaded from the MDI homepages. The CR synoptic charts from MDI have two forms: magnetic field and intensity synoptic charts. Only the magnetic field charts are used in this paper. They are generated from the MDI magnetograms at level 1.8. They are well re-calibrated, and several observations of every location which have been collected over the course of a solar rotation (~ 27 days) are averaged to make up the charts. Therefore, the strength of the magnetic field at each synoptic grid point is averaged, and they have been corrected by the differential rotation before. Through the averaging process, the effects of cosmic rays have also been reduced. The projection effect of the magnetic field have been corrected by assuming that MDI makes line-of-sight measurements of a radial magnetic field. Finally, the correction to the pixel area has also been performed in this paper with a scaling factor (see., Berger & Lites, 2003; Tran et al., 2005; Ulrich et al., 2009).

The finally synoptic charts of the magnetic fields have two versions of the maps: a radial and a line-of-sight (LOS) version. The synoptic charts about the projection effect along the longitude are much better than the snapshot magnetograms, but they have lost the temporal resolution. The noise level of the synoptic charts is about 5 Gauss, and the resolution of the synoptic charts have been changed to a 3600×1080 pixel synoptic map. The carrington longitude is linear, while the carrington latitude is sine. Noting that the data at each longitude in these synoptic charts is observed at different time, so the longitude in the synoptic charts is also represent the time information.

All the synoptic maps, whether the radial or the LOS are constructed from the data which observed by the disk meridians. These maps used the data that observed near central meridian (0°) are called

ordinarily synoptic charts, and additional charts are using the data from other disk meridians, such as 60°E , 45°E , 30°E , 15°E , 15°W , 30°W , 45°W , and 60°W . However, those additional charts have the disadvantage of disk longitude offsetting, the ordinarily synoptic charts have not, so only the ordinarily synoptic charts are used in this paper. Therefore, only the LOS magnetic field observed near central meridian for Carrington Rotation synoptic charts are used to identified the BMRs. Figure 1 (a) shows an example of the synoptic images which we use in this paper.

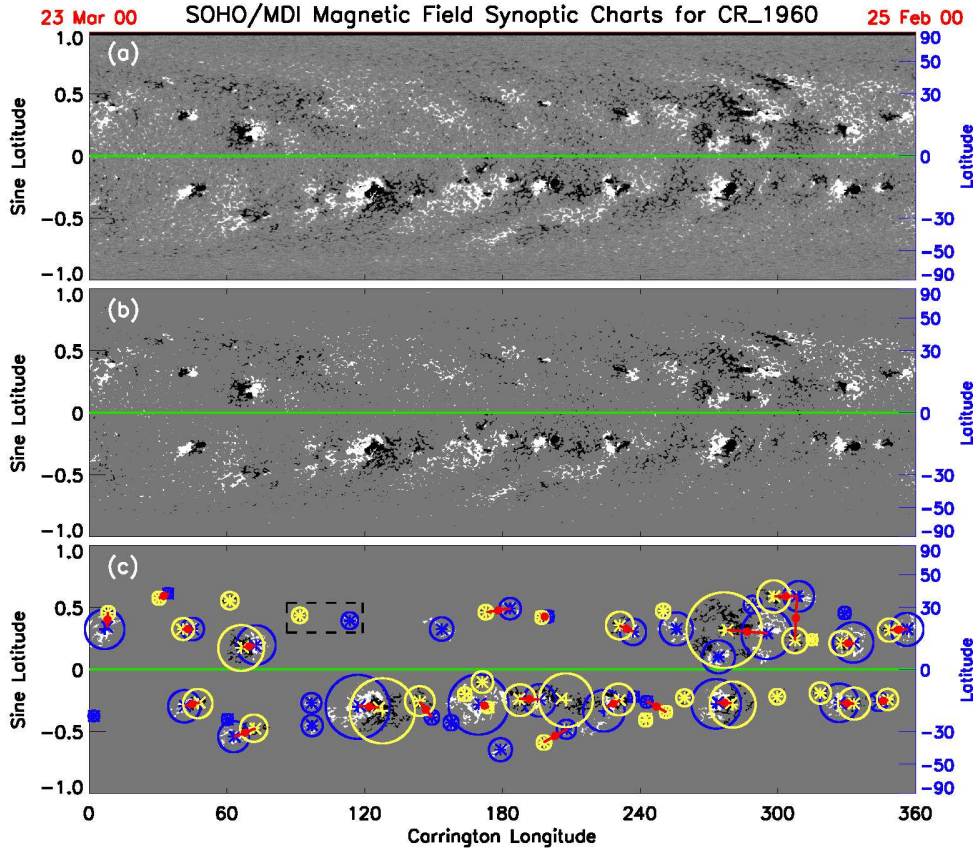


Fig. 1 (a): The LOS magnetic field Synoptic Charts for Carrington Rotation 1960 near central meridian, which started on 25 February 2000 and ended on 23 March 2000. (b): The magnetogram after subtracting the strength threshold from panel (a); (c): The magnetogram after subtracting the area threshold from panel (b), the blue and yellow circles are the positive and negative poles, while the ‘+’ and ‘×’ represent the geometric centers and the flux-weighted centers, respectively; the identified BMRs are connected with the red lines, the filled circles are the positions of the BMRs. The green line in each panel represents the solar equator.

2.2 Data reduction

Two magnetic poles of the BMRs in the active regions are defined by the threshold method, which include the strength and area thresholds. As illustrated in Figure 1, there are essentially two steps, each of which corresponds to one panel in this figure. The first step is to define the magnetic poles of the

BMRs. The positive and negative magnetite fields are separated from the observation data, and the two magnetic poles are identified respectively. Then we determine the strength threshold of the positive or negative magnetic filed for every magnetogram with equation (1). However, the magnetograms used in this paper are from May 1996 to December 2010, which included the whole 23rd solar cycle and the beginning phase of 24rd solar cycle. The strength thresholds with equation 1 for different phases of the magnetograms have large difference. To rule out this difference, we take the average value (\overline{TH}) of all thresholds, and this value is 55 G for the positive filed and -55 G for the negative field. This value is similar to that used by Zhang et al. (2010), who have been identified the ARs by the minimum magnetic filed of 50 G with SOHO/MDI synoptic magnetograms. Figure 1 (b) gives the results after subtracting the \overline{TH} from the original observation data.

$$TH = \mu \pm \gamma \cdot \sigma, \quad (1)$$

In equation (1), μ is the mean value, and σ represents the standard deviation, while γ is a constant which determines empirically based on the type features to be detected. In this paper we set $\gamma = 2$, which is same as Colak & Qahwaji (2008) to determine the magnetic polarities of ARs. While '+' is for the positive filed and '-' is for the negative filed.

Next, we will identify the two poles of the BMRs by the area threshold. The magnetic images have been separated several individual unconnected regions after subtracting the strength threshold, and these regions can be marked automatically by the code of LABEL_REGION.pro in Interactive Data Language (IDL). However, these isolated regions are not considered as the magnetic poles, for these isolated regions which close to each other may be the same magnetic pole. Therefore, we have to determine the area of the magnetic poles. That is to say, it is possible that these closer regions belong to the same magnetic pole. So the positions (geometric centers) and the equivalent diameters (consider the isolated region as a circle) of these isolated regions have been calculated; and for every isolated region, we regard the geometric center as the reference point and two times equivalent diameters as edge length to draw a square box. If these square box have the overlapping regions, they belong to one magnetic pole, otherwise they belong to the different magnetic poles. Thus these closer isolated regions may be one magnetic pole. But not all of the magnetic poles could be the real poles of the BMRs in this paper. These poles which have small area are possible not to be the real poles of the BMRs in the active regions, because we mainly study the larger and stronger BMRs here. Therefore, the small magnetic poles have to be ruled out. The minimum area used here is similar to previous studies. For example, Harvey & Zwaan (1993) studied the area of BMRs larger than 2.5 square degrees ($\sim 373 \text{ Mm}^2$); Tang et al. (1984) had detected the ARs as small as 450 Mm^2 ; the smallest area studied by Schrijver (1988) was 310 Mm^2 ; Wang & Sheeley (1989) even studied the ARs as small as about 200 Mm^2 . Based on these values, we define the area (A) threshold as 250 pixel^2 ($\sim 495 \text{ Mm}^2$) in this paper. In other words, these regions with the total area less than 250 pixel^2 are excluded as the magnetic poles. Figure 1 (c) shows the positive (blue circles) and negative (yellow circles) poles in Carrington Rotation 1960, the plus ('+') and cross ('x') represent the geometric center and the flux-weighted center, respectively. And we consider the flux-weighted centers as the positions of the magnetic poles. For each magnetic pole (positive or negative), we also calculate their radius (R), fragment number (N), magnetic field (B), magnetic flux (F), and magnetic flux density (f). Here, the magnetic pole is supposed to be a circle. The fragment number is the amounts of the isolated regions in the magnetic pole, and the magnetic field is maximum value of the magnetic pole. The magnetic flux is the total value of the magnetic pole, while the magnetic flux density is the mean value of the magnetic filed.

The second step is to identify the BMRs from the identified positive and negative poles. In this paper, we assume that BMRs are formed by the closest magnetic poles with opposite polarity, but the BMR direction in northern is opposite from that in southern hemisphere. In the northern hemisphere, a BMR is defined as a negative pole to link the closest positive pole; while in the southern hemisphere, the positive pole is used to link the closest negative one, such as the red lines linking the two magnetic poles in Figure 1 (c). The distance (D) between the positive and negative poles of each BMR is measured, and the ratio of D/R is shown in Figure 2. There is a normal distribution of D/R, and the maximum

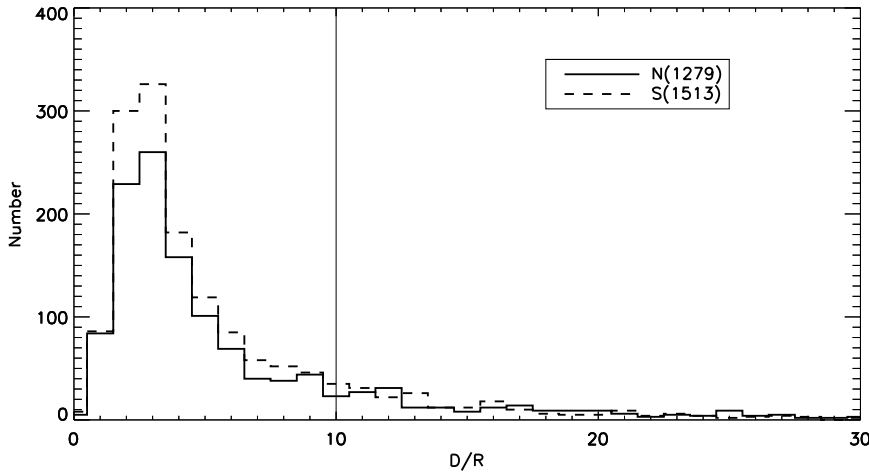


Fig. 2 The ratio between the distance (D) and the radius (R) of the magnetic poles in northern (solid line) and southern (dash line) hemispheres, respectively.

value is around 3. These BMRs with a big value of D/R , such as greater than 10, indicating a large distance between positive and negative poles with a small area size, are possible not real. Therefore, these BMRs with $D/R \geq 10$ (the vertical line in Figure 2) are ruled out to analyze in this paper, i.e., the one marked with the rectangle. Namely, a positive pole linking with the negative one with a shortest area-weight distance is identified as a BMR in the southern hemisphere. And the same rule is applied in the northern hemisphere. The red lines in Figure 1 (c) link the identified BMRs, the filled circles represent the positions of the BMRs, which are the middle positions of the positive and negative poles of the BMRs.

3 RESULTS

Using the method mentioned in Section 2.2, we analyze the SOHO/MDI data from Carrington rotation 1909 (May 1996) to 2104 (December 2010). This period covers the whole 23rd solar cycle and the beginning phase of 24rd solar cycle. There are 4 MDI images (CR1938, CR1939, CR1940 and CR1941) missing due to the malfunction of the SOHO in 1998. Some MDI images (e.g., CR1937, CR1944, CR1945, CR1956, CR2011, CR2015 and so on) are partial, but they are enough for our analysis. Finally, 2948 positive poles and 2940 negative poles are identified from these MDI images, and 2234 BMRs are identified, 1005 of them are located in northern hemisphere, while the other 1229 are located in southern hemisphere. However, there are 3171 NOAA ARs published during the same period. Such difference is mainly because that only these LOS magnetic fields observed near central meridian are used. The criterion to identify the BMRs and NOAA ARs is also different.

3.1 The positions of BMRs

In our study, each BMR has its own latitude and time. On the MDI synoptic image, the midpoint of the positive and negative poles is marked as the BMR position, which is the function of the latitude and time. Figure 3 (a) shows the distribution of the BMR latitudes. Most (95.7%, 2138/2234) of the BMRs are located in the low latitude in the solar disk, i.e., between -30° and 30° ; while only 4.3% (96/2234) BMRs are exceed this range but not higher than $\pm 50^\circ$. Here, '+' and '-' represent the latitudes of the BMRs which located in the northern and southern hemispheres, respectively. This is consistent well

with the ARs and sunspots, which are also typically located at the low latitude in the solar surface. The mean values of the BMR latitudes are 16° and -16° in northern and southern hemispheres, respectively. Panel (b) further gives the BMR latitudes in solar disk varying with solar cycles, it appears similar as the butterfly diagram described by Maunder (1904, 1922), which explained as the emergence positions of the ARs (or sunspots) progressively drifting toward the solar equator (Hathaway et al., 2003). And this further confirms that the BMRs in this paper are essentially bipolar fields.

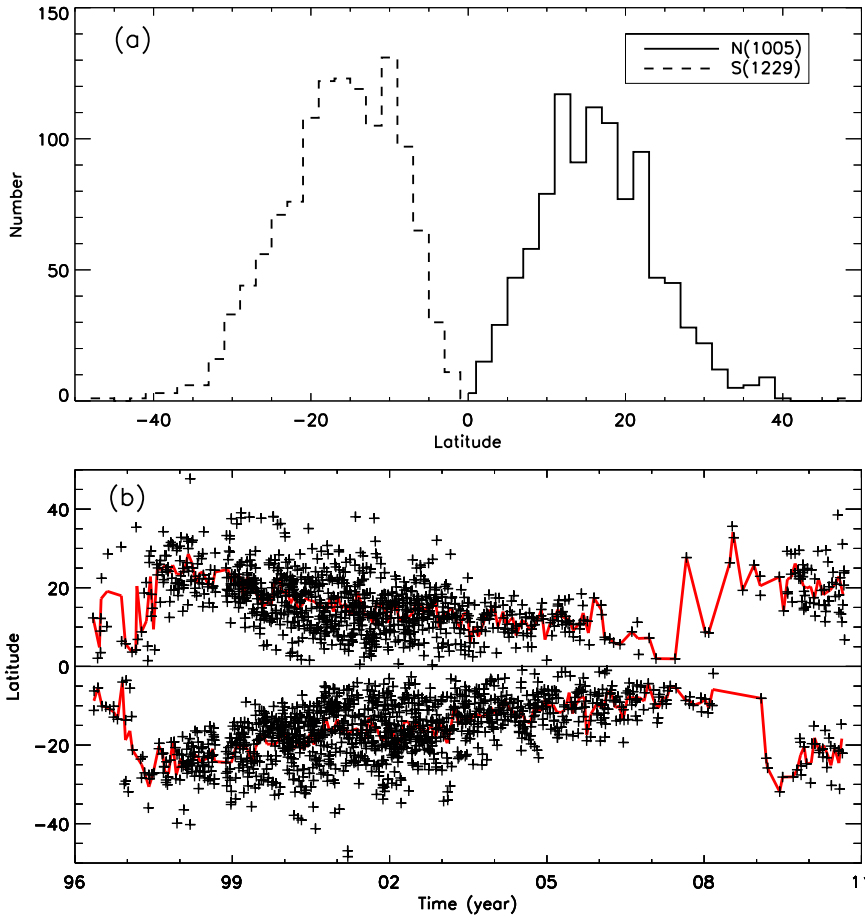


Fig. 3 (a): The distribution of BMR latitudes in northern (solid line) and southern (dash line) hemispheres, respectively. (b): The distribution of BMR latitudes with solar cycles, and the two red lines show the flux-weighted centers of BMRs per Carrington rotation for the two solar hemispheres.

3.2 The parameters of the BMRs

For these identified BMRs, we statistical study their separations (D_S), fragment number (N), area (A), magnetic field (B), magnetic flux (F), magnetic flux density (f). The separations are the distance between the positive and negative poles of the BMRs, and the fragment number, area and magnetic flux are

Table 1 Statistical results of the BMRs and ARs.

Parameter	Mean			Median			Min			Max		
	BMR	AR1	AR2	BMR	AR1	AR2	BMR	AR1	AR2	BMR	¹ AR1	² AR2
D_S (Mm)	112	-	-	100	-	-	3.2	-	-	448	-	-
N	26	7.8	8	19	5	4	2	1	0	168	69	90
A (10^{19} cm ²)	8.8	6.1	0.3	5.5	3.5	0.06	1.0	0.3	0	79.7	68	6.9
B (G)	1194	-	-	1107	-	-	252	-	-	2972	-	-
f (Mx cm ²)	117	-	-	109	-	-	58	-	-	339	-	-
F (10^{21} Mx)	22.4	16.7	-	12.3	8.4	-	1.7	0.9	-	243	197	-

Notes: ¹AR1: the parameters of active regions are cited from Zhang et al. (2010).
²AR2: the parameters of active regions are from the NOAA manual catalog.

the sum of absolute values for positive and negative poles of the BMRs, while the magnetic field and magnetic flux density are the half of the total absolute values for positive and negative poles of the BMRs. The statistical results are shown in Figure 4 and 5. While table 1 and 2 also list these parameters in the documents to compare with the previous findings. Here AR1 and AR2 are the active regions which identified from the different definitions, i.e., AR1 is the active region identified by Zhang et al. (2010) based on their automated method, while AR2 is the active region defined from the NOAA manual catalog.

Figure 4 shows the distribution of each BMR parameter, and their typical values are listed in table 1. The separated distances (D_S) range from 3.2 Mm to 448 Mm, which is shown in panel (a). The largest separation in this paper is greater than the value of 26 deg (~ 320 Mm), which obtained by Howard (1989). But the number of such large separation is very rare, for example, only 1 separation of the BMR exceeds 400 Mm, while only 0.9% (20/2234) separation of the BMRs exceed 300 Mm. The mean separation distance of these BMRs is 112 Mm, which is similar to the value of 86 Mm (Howard, 1989). The fragment number (N) of these BMRs are from 2 to 168, and the average number of them are about 26, which is shown in panel (b). From panel (a) and (b), we can see that the distribution is similar to that of the separation distances, the larger number is very less, only 1.9% (42/2234) are greater than 100. The same results are applied to the distribution of the BMR flux density, as shown in panel (d). The minimum flux density is 58 Mx cm⁻², the maximum flux density is 339 Mx cm⁻² and the average flux density is 117 Mx cm⁻², while only 0.45% (10/2234) of them exceed 250 Mx cm⁻². However, the distribution of the BMR magnetic field is different. As shown in panel (c), there are two peaks in the distribution of the magnetic field, one is about 600 G, the other is around 1500 G, and the magnetic strength ranges from 252 G to 2972 G.

For these 2234 BMRs, their area and magnetic flux are also measured. The area of these BMRs ranges from 1.0×10^{19} cm² (~ 1000 Mm²) to 7.97×10^{20} cm² ($\sim 7.97 \times 10^4$ Mm²). The smallest area of BMRs in this paper is larger than previous results of 300–400 Mm² for the ARs (Tang et al., 1984; Schrijver, 1988; Harvey & Zwaan, 1993; Zhang et al., 2010), and the largest area is also greater than the earlier results of about $(1-7) \times 10^4$ Mm² for the ARs (Tang et al., 1984; Schrijver, 1988; Wang & Sheeley, 1989; Harvey & Zwaan, 1993; Zhang et al., 2010). The flux of these BMRs are from 1.7×10^{21} Mx to 2.43×10^{23} Mx, which is similar to the AR flux from 8.6×10^{20} Mx to 1.97×10^{23} Mx obtained by Zhang et al. (2010), but the maximum value is larger than earlier results of about 10^{22} Mx for ARs (Howard, 1989; Wang & Sheeley, 1989). Then the frequency distributions of these BMRs occurrence as functions of flux and area are shown in the two bottom panels of Figure 4. It is hard to say that the behaviors of the frequency distributions for the whole area and flux. However, using the maximum likelihood estimation (MLE) method developed by Clauset et al. (2009), both the BMR area and flux exhibit a power-law behavior, i.e., $dN/dx \propto x^{-\alpha_x}$. The MLE method is based on the Kolmogorov-Smirnov statistic to determine the lower cutoff (x_{min}) of the power-law behavior, which is marked by the dashed lines in panel (e) and (f). Using the MLE method, we obtain the power-law index of $\alpha_F = 1.93 \pm 0.05$ for the BMR flux and $\alpha_A = 1.98 \pm 0.06$ for the BMR area. This is consistent well with the power-law distribution of the large solar activities, such as radio bursts, soft X-rays, hard X-rays, interplanetary

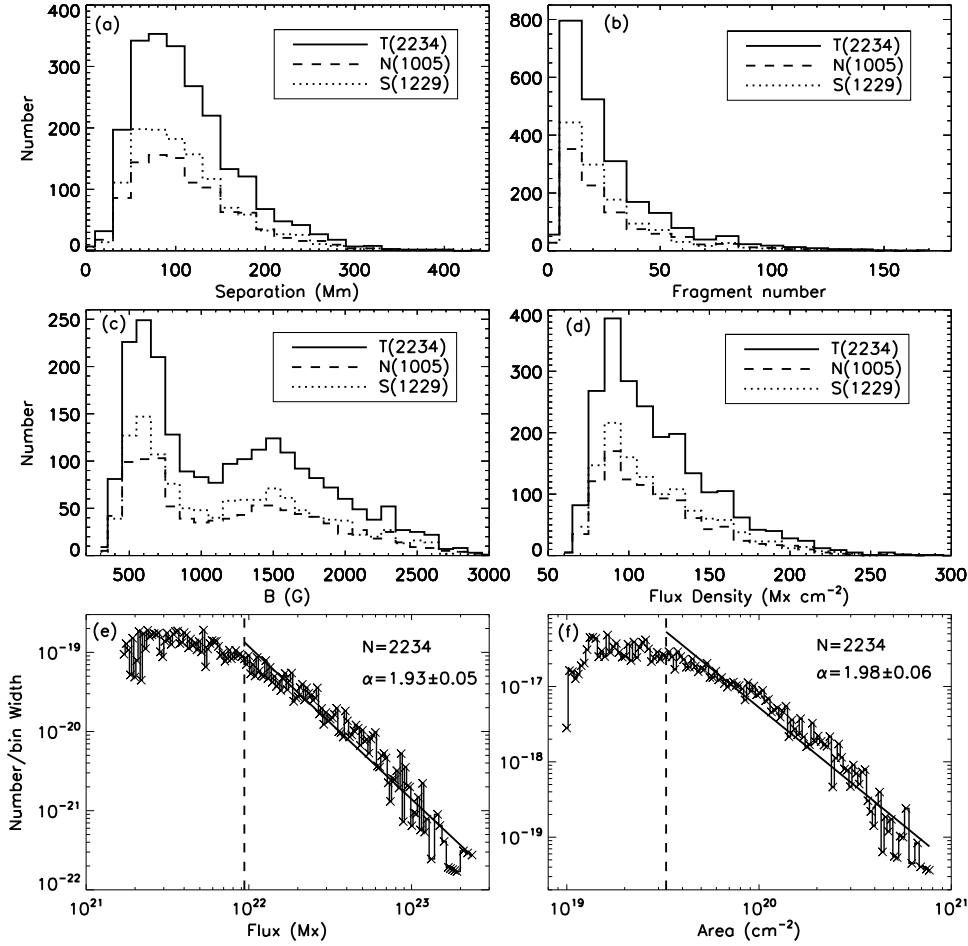


Fig. 4 The solid profiles are the distributions of the BMR separated distances (a), fragment number (b), magnetic field (c), magnetic flux density (d). The dashed and dotted profiles represent the BMR parameter distributions in northern and southern hemispheres, respectively. The other two panels are the distribution of the BMR flux (e) and area (f) in log-log space.

type III bursts, interplanetary particle events and CMEs (Crosby et al., 1993; Aschwanden et al., 1998). Dennis (1985) and Crosby et al. (1998) further summarize α_x for the distributions of different flare-related parameters and state that it varies from 1.4 to 2.4. This is also proved by many authors for solar flares (Wheatland, 2000; Su et al., 2006; Li et al., 2012), CMEs (Wheatland, 2003), radio bursts (Ning et al., 2007; Song et al., 2012) and other small-scale magnetic fields (Parnell et al., 2009; Li et al., 2013). In our results, $\alpha_A = 1.98 \pm 0.06$ for the area of the BMRs are followed by the fractal models (Aschwanden & Parnell, 2002). While $\alpha_F = 1.93 \pm 0.05$ for the BMR flux are consistent with the index of coronal activities (i.e., solar flares, CME, radio burst) and bright points (Li et al., 2013). Our findings indicate that there are not fundamental differences for their generation in solar atmosphere, whatever the (small or large) scale or the (low or high) height above solar surface. And the observations also show that both the coronal activities and bright points are strongly related to the magnetic fields, indicating the common features of the generating magnetic structures at small or large scales.

Table 2 Statistical results of the BMRs vs ARs per Carrington rotation.

Parameter	Mean			Median			Min			Max		
	BMR	AR1	AR2	BMR	AR1	AR2	BMR	AR1	AR2	BMR	¹ AR1	² AR2
N_0	11	11	13.5	10	8	11	0	0	0	35	37	39
N	312	85	126	210	55	101	0	0	0	1265	327	413
A (10^{20} cm ²)	10.2	6.7	0.5	5.4	4.3	0.3	0	0	0	44.0	26.7	1.8
B (10^3 G)	1.39	-	-	1.07	-	-	0	0	0	4.19	-	-
f (10^3 Mx cm ²)	1.37	-	-	1.13	-	-	0	0	0	4.19	-	-
F (10^{23} Mx)	2.6	1.8	-	1.4	1.3	-	0	0	-	10.5	6.96	-

Notes: ¹AR1: the parameters of active regions are cited from Zhang et al. (2010).

²AR2: the parameters of active regions are from the NOAA manual catalog.

Figure 5 displays the variation of BMR parameters per carrington rotation with the period from 1996 to 2010. The typical values of these BMR parameters per Carrington rotation are listed in table 2. Here N_0 is the number of the BMRs or ARs per carrington rotation, the other symbols is same as in table 1. As shown in Figure 5, there are double peaks during solar maximum. And if we examine carefully the panels (c), (d) and (e), we could find that the second peak flux (in late 2001) of BMRs are mainly caused by the large area of the emerged BMRs, but not the mean strength of the magnetic field. Based on this, the 23rd solar cycle is peaked in late 2001 but not in early 2000. These results are consistent well with previous findings (Zhang et al., 2010). From table 2 we can see that the BMR parameters are consistent well with the AR parameters except for the fragment number. In Figure 5, we also plot the BMR parameters vary with solar cycles in the northern (blue dashed line) and southern (red dashed line) hemispheres, which clearly show the north-south asymmetry of the BMR distribution. And this north-south asymmetry is also shown in panels (a) – (d) of Figure 4. Similar north-south asymmetry of ARs has been reported earlier (Temmer et al., 2002; Zharkov & Zharkova, 2006; Zhang et al., 2010). However, this asymmetry is not well understood yet. We also plot the parameters of positive (blue solid line) and negative (red solid line) poles vary with solar cycles, and the positive and negative parameters of the BMRs are almost the same during the solar cycles, although there may be some difference in one or two carrington rotation periods. In table 2, the parameters of the BMRs and ARs are zero in solar minimum, whether in our data or in other data. This is because that the chance of appearing ARs is very small or even not in one carrington rotation during solar minimum.

3.3 The orientation of BMRs

The orientation angles of the ARs are important to understand the solar cycles and have been studied in the past (e.g., Wang & Sheeley, 1989; Howard, 1989, 1991a). However, most of the data they used are fully-disk magnetograms which observed on ground. In this paper, we use the MDI carrington rotation charts to study the orientation angles. Figure 6 gives the definition of the orientation angle (θ) of BMRs in northern and southern hemispheres, respectively. In northern hemisphere, the orientation angle (θ) is defined to be the angle of vector originating in the flux-weighted center of the positive pole and rotating clockwise and terminating in the flux-weighted center of the negative pole; while it is defined to be the angle of vector originating in the flux-weighted center of the negative pole and rotating anti-clockwise and terminating in the flux-weighted center of the positive pole in southern hemisphere. Noting that we separately define the BMR orientation angle in northern and southern hemisphere. Both the BMR orientation angles in northern and southern hemispheres range from -90° to 270° . In this paper, the normally oriented BMRs refer to those BMRs whose orientation angles range from -90° to 90° , while the abnormal orientation angles are between 90° and 270° in solar disk, whatever in northern hemisphere or in southern hemisphere.

Figure 7 gives the orientation angle (θ) distribution of these BMRs with a bin of 10° in northern (solid lines) and southern (dashed lines) hemispheres, respectively. Panel (a) shows all the BRMs are

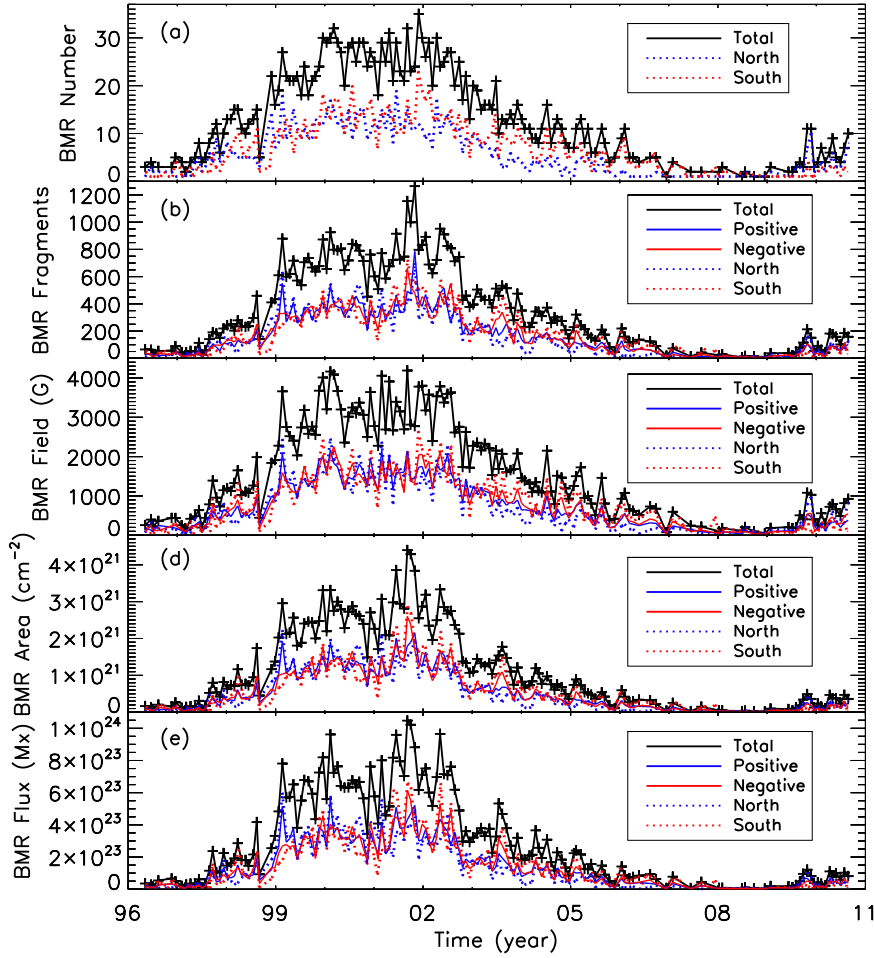


Fig. 5 The BMR parameters per Carrington rotation with time from 1996 to 2010. (a): the BMR number (black); (b): the BMR total fragment number (black), positive fragment number (blue), and negative fragment number (red); (c): the BMR total magnetic field (black), positive magnetic field (blue), and negative magnetic field (red); (d): the BMR total area (black), positive area (blue), and negative area (red); (e): the BMR total flux (black), positive flux (blue), and negative flux (red). The dotted profile shows the parameters in northern (blue dashed) and southern (red dashed) hemispheres.

from carrington rotation 1909 to 2104, including the whole 23rd solar cycle and the beginning phase of 24rd solar cycle. Since the orientation angles are ranging from -90° to 270° and most of them are focus on around 0° or 180° . In this paper, the median values of the whole data are 13° and 11° in northern and southern hemispheres, respectively, indicating that whether in northern hemisphere or southern hemisphere, the orientation angles of the BMRs are slightly deviated to the solar equator direction. In panel (a), we can see that there are two peaks in both northern and southern hemispheres. And there are much more BMRs around 0° than that around 180° . Then we separated the BMRs into the entire 23rd solar cycle (from CRs 1909 to 2070) and the beginning phase of 24rd solar cycle (from CRs 2071 to 2104), as shown in panels (b) and (c). From which, there is only one peak whether in northern or

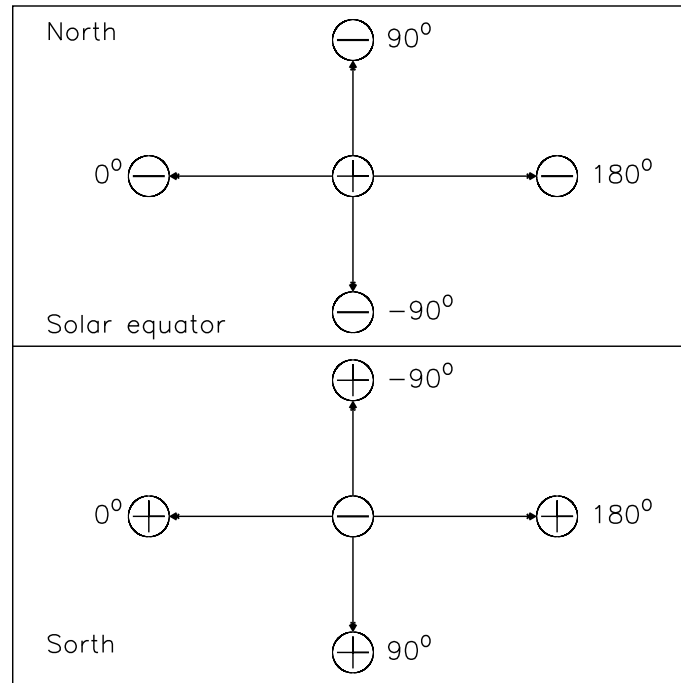


Fig. 6 Schematic representation of the orientation angle (θ) of the BMRs. In northern hemisphere the positive pole ('+') is the angle center, and the negative pole ('-') rotation clockwise; while in southern hemisphere, the negative pole is the angle center, and the positive pole rotation counter-clockwise. The angle ranges from -90° to 270° .

southern hemispheres at the entire 23rd solar cycle, and the median values of the BMR orientation angles are 11° and 10° in northern and southern hemispheres, which is similar to that of all the data. And at the beginning of 24rd solar cycle, there is also one peak both in northern and southern hemispheres, but the median values of the BMR orientation angles are 187° and 181° in northern and southern hemispheres, respectively. These results suggest that the two peaks of the orientation angles in panel (a) are from the 23rd and 24rd solar cycles, respectively.

Our results show that the orientation angles of the BMRs are generally slightly deviated to the solar equator direction (panel (a) in Figure 7), and that the directions of the BMRs are opposite in northern and southern hemispheres (panel (a) in Figure 7), and that the magnetic polarity of BMRs is reversed in solar minimum of the solar cycle (panel (b) and (c) in Figure 7). These results are also shown in Figure 8, which gives the variation of BMR orientation angles with respect to the phase of solar cycles from May 1996 to December 2010. The squares and triangles represent the BMRs located in the northern and southern hemispheres, respectively. In this figure, the BMR orientation angles vary with solar cycles, and the polarities of BMRs are changing in different solar cycles. We note that the orientation angles are reversed around in June 2008. That is to say, the 23rd solar cycle is from 1996 to 2008, and the duration is about 12 years. This perhaps can be explained by the extended activity cycle, because the sunspot region of a new solar cycle could begin to appear as much as ~ 1.6 years before the defined solar minimum and continue to emerge up to ~ 1.8 years after the following minimum. These results are consistent well with the previous findings about the ARs (Howard, 1989; Wang & Sheeley,

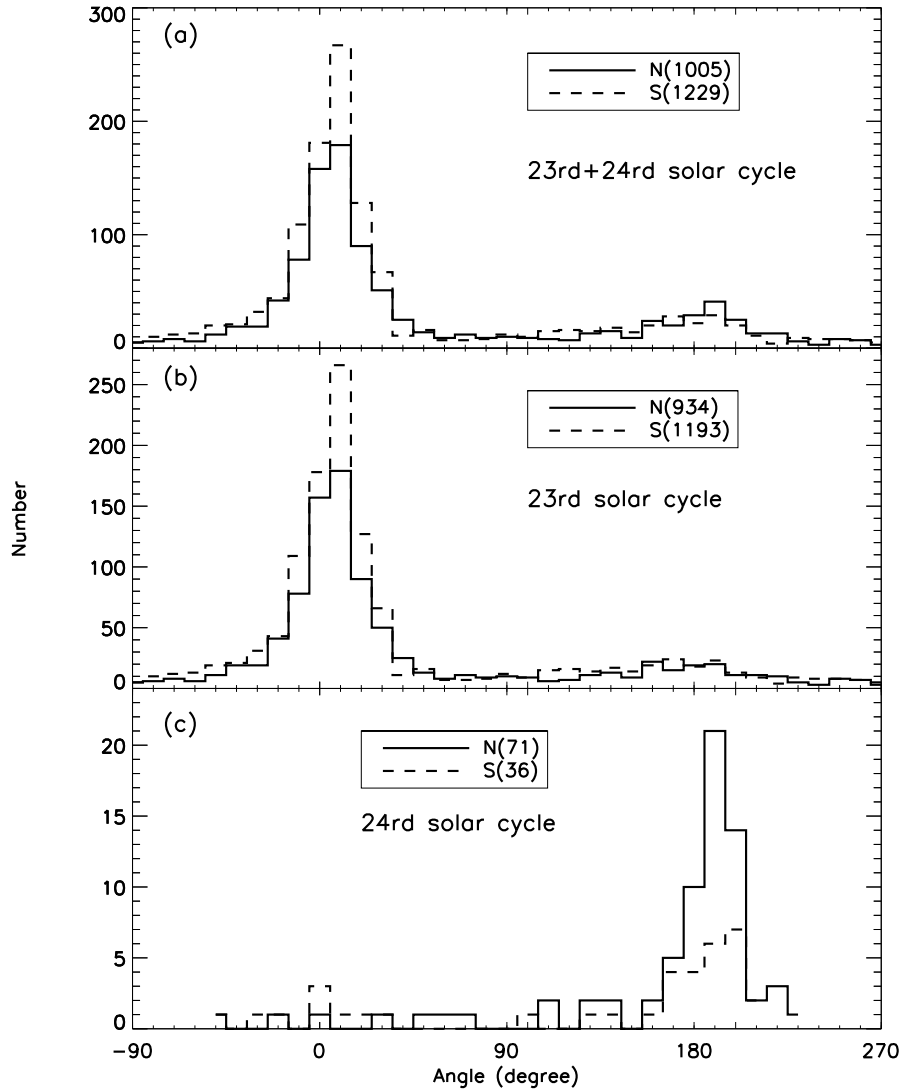


Fig. 7 The BMR orientation angle (θ) distribution with a bin of 10° from the data during the 23rd and 24rd solar cycle (a), from the data during the 23rd solar cycle (b) and from the data during the beginning of 24rd solar cycle (c). While the solid and dashed lines represent the BMRs in northern and southern hemispheres, respectively.

1989; Howard, 1991a) and sunspots (Maunder, 1904; Hale et al., 1919; Howard, 1991b), indicating that all the large-scale phenomena related to the bipolar magnetic fields are following by the “Hale’s Polarity Laws”. That is to say, during the first solar cycle the positive poles of the BMRs are the leading polarity in northern hemisphere and the negative poles of the BMRs are the leading polarity in southern hemisphere; while in the next solar cycle, the BMR polarity is reversed, the leading polarity are negative poles in northern hemisphere and positive poles in southern hemisphere.

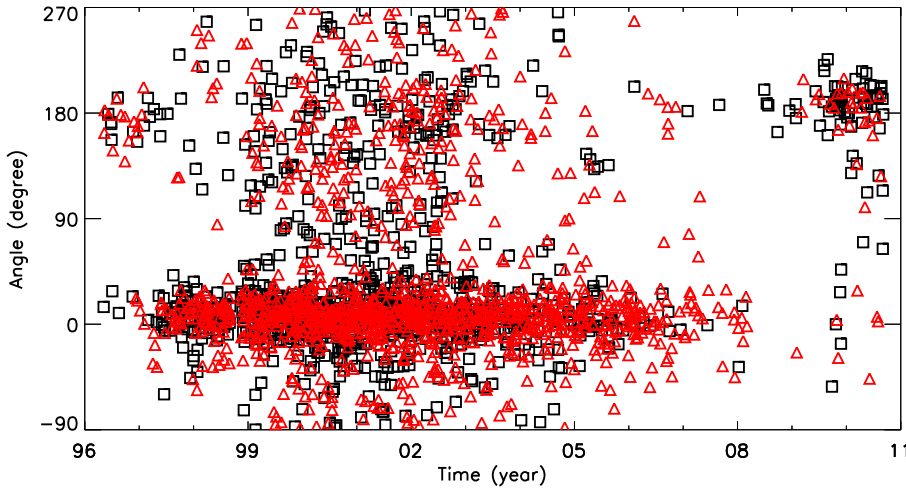


Fig. 8 The time evolution of the BMR orientation angles (θ) from May 1996 to December 2010 in northern (squares) and southern (triangles) hemispheres.

Figure 9 displays the BMR orientation angles dependence on their latitudes (a), magnetic filed (b), separations (c), area (d), fragment number (e), total flux (f) (the sum values between the absolute positive and negative flux), flux density (g) and net flux (h) (the minus values between the absolute positive and negative flux). It is hard to see any relationship between the orientation angles and other parameters in the BMRs, especially between the orientation angles and their latitudes. Here all of the 2234 BMRs are analyzed, including the normal and abnormal BMRs from May 1996 to December 2010. Then only the BMRs (2127) during the 23rd solar cycle are selected to analyze, regardless of the northern or southern hemispheres in solar disk. Figure 10 gives the average parameters for various values of orientation angles of these 2127 BMRs. The BMRs with larger absolute orientation angles tend to show greater deviation on average values of parameters (e.g. separations (a), area (b) and flux (c)) than those with smaller absolute orientation angles. Especially for these normal orientated BMRs whose orientation angles between -50° and 50° (dotted lines), their deviation and fluctuation are much smaller than other BMRs. However, the net flux of these normal orientated BMRs whose orientation angles between -50° and 50° (dotted lines) are always smooth and the fluctuation are very small (panel d). But for those other orientated BMRs (the absolute orientation angles are exceeded 50°), their fluctuation and deviation are much larger. These results are similar to that obtained from the ARs by Howard (1989, 1991a), who found that these ARs with less absolute orientation angles tend to show smaller deviation. Finally the magnetic flux of the BMRs in this paper are larger about one magnitude than others, which possibly due to the resolution and sensitivity of the different instruments. Howard (1989) have been said that the inherent disadvantage of their data is the poor resolution, and this is the advantage of our data as the MDI magnetic charts have high resolution and high sensitivity.

Based on the above analyzing, only the normal BMRs 1543 which the orientation angles range from -50° to 50° in 23rd solar cycle are selected to analyze, regardless of the northern or southern hemisphere on solar disk. Figure 11 shows the orientation angles dependence on the absolute latitudes for these 1543 normally oriented BMRs during the 23rd solar cycle, the average orientation angles are taken over 2.5 degree latitudes, and the error bars represent the standard deviations of these mean values. For these normally oriented BMRs, the orientation angles increase with their latitudes on the whole. This is consistent well with the results that the tilt angles of the ARs and sunspots general increasing with the latitudes (e.g., Hale et al., 1919; Wang & Sheeley, 1989; Howard, 1989, 1991a,b). And at the latitudes

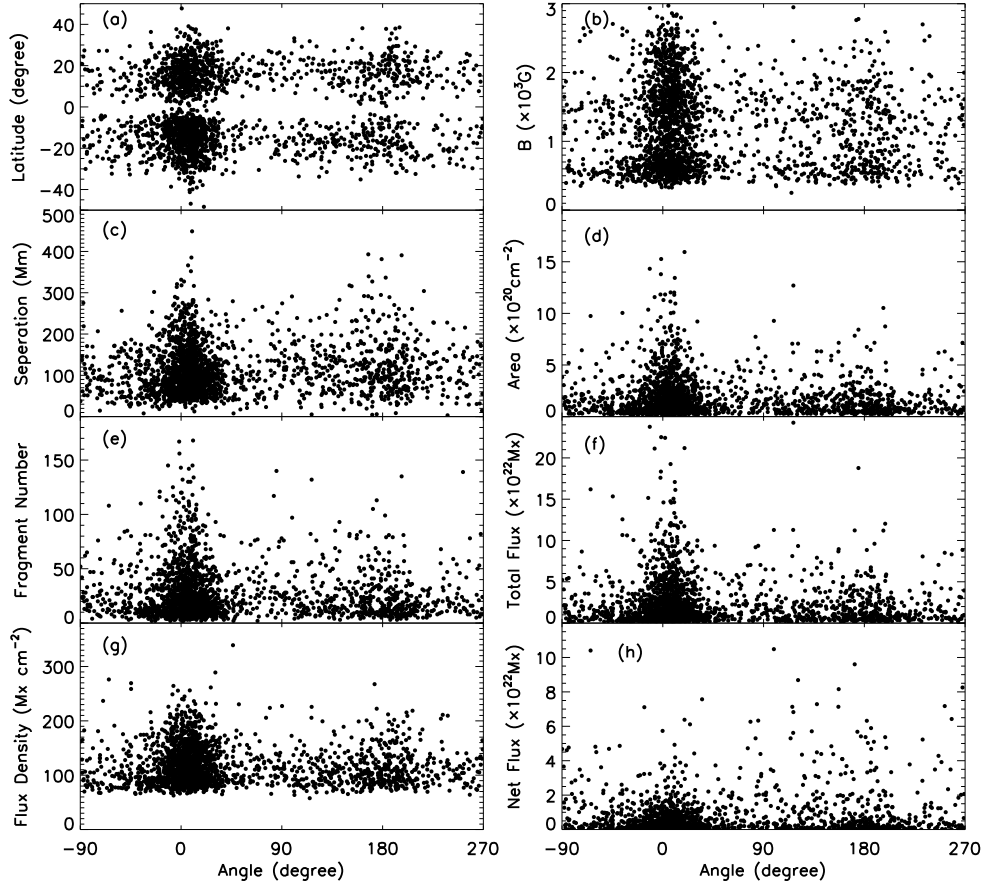


Fig. 9 The BMR orientation angles (θ) dependence on their latitudes (a), magnetic field (b), separations (c), area (d), fragment number (e), total flux (f), flux density (g) and net flux (h).

equator-ward of about 5 degree, the orientation angles show the negative values on average but not very significant, which is also similar to the results from the tilt angles of ARs (Howard, 1991a).

4 CONCLUSIONS AND DISCUSSIONS

Using SOHO/MDI LOS magnetic data from CRs 1909 to 2104, we statistically study the observational features of BMRs. To obtain the BMRs, we firstly identify the positive and negative poles with the strength and area thresholds, respectively; then using the criteria of closest area-weight distance between positive and negative poles to determine the BMRs. Finally, 2234 BMRs are obtained from the observation data, 1005 of them are lactated in northern hemisphere and the other 1229 BMRs are lactated in southern hemisphere.

For these BMRs, the average latitudes are 16° and -16° in northern and southern hemispheres, respectively. And most (95.7%) of these BMRs locate between -30° and 30° , while only a little (4.3%) BMRs locate in high latitude but not exceed 50° . The time variation of these BMR latitudes with solar cycles is similar to the classical butterfly diagram of sunspots (Maunder, 1904, 1922). These BMRs are

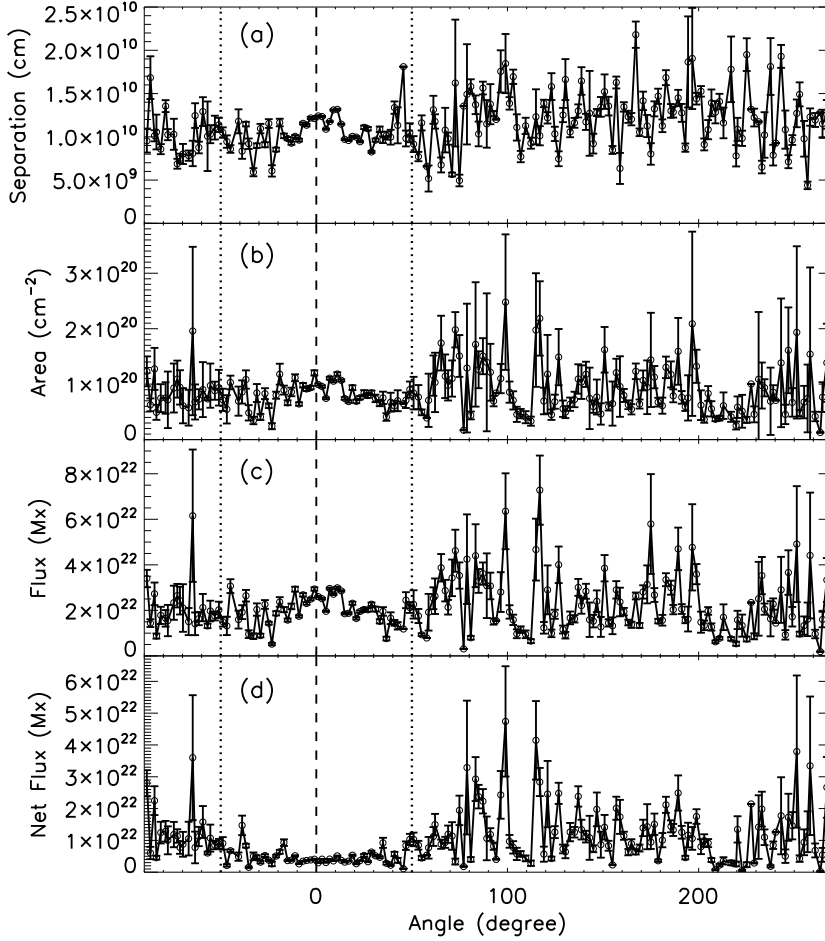


Fig. 10 The average BMR parameters (separations (a), area sizes (b), total magnetic flux (c) and net magnetic flux (d)) for 2 degree intervals of BMR orientation angles. The error bars represent the standard deviations of those mean values, and the dashed lines are corresponding these mean values with 0 degree, while the dotted lines corresponding these mean values with -50 or 50 degree.

also follow the “Spörer’s Law”. The BMR separations, area, flux are calculated (see table 1 and Figure 4) and are similar to the results obtained by Zhang et al. (2010). However, the fragment number is much larger than others, this is because that we do not limit the area size of the fragments. The variation of BMR parameters per carrington rotation with solar cycles is also studied in this paper, and we further confirm that the 23rd solar cycle peaked in late 2001 but not in early 2000, this is consistent well with the results obtained by Zhang et al. (2010). We also find the north-south asymmetry of the BMRs, which is similar to previous findings about the north-south asymmetry of the ARs (e.g., Temmer et al., 2002; Zharkov & Zharkova, 2006; Zhang et al., 2010; Shetye et al., 2015).

We find that the frequency distributions of these 2234 BMRs as function of magnetic flux and area exhibit a power-law behavior, and the power-law indexes, $\alpha_F = 1.93 \pm 0.05$ for the magnetic flux, $\alpha_A = 1.98 \pm 0.06$ for the area, which are consistent with the previous findings for the large-scale coronal

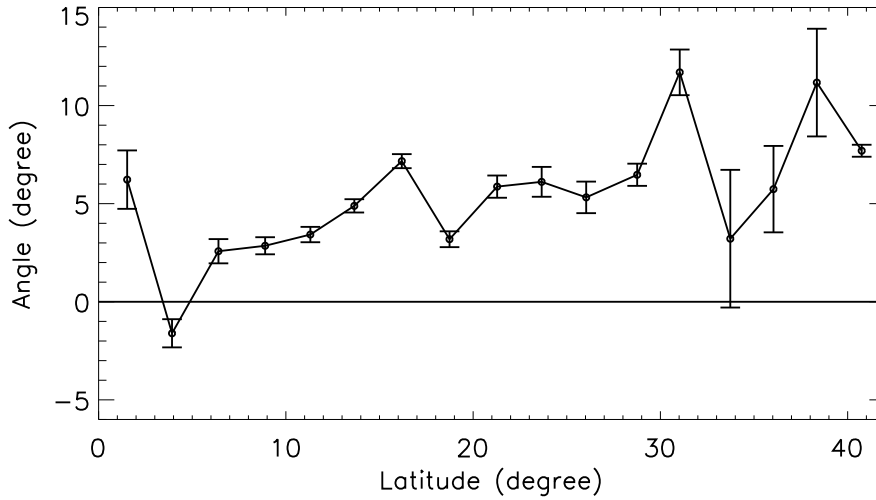


Fig. 11 Average BMR orientation angles for various intervals of absolute solar latitudes in degrees. The average values are taken over 2.5 degree latitudes, the error bars represent the standard deviations of those mean values.

activities (e.g., solar flares, CMEs, radio bursts) and small-scale magnetic elements (Li et al., 2013). This suggests that the area size of the BMRs are followed by the fractal models (Aschwanden & Parnell, 2002) and the mechanisms of the surface magnetic features on the Sun are free of scales, indicating that all the surface magnetic features, regardless of their scales, are generated by the similar mechanisms, or indicating that the surface processes (i.e., fragmentation, coalescence, cancelation and so on) in a way which lead to a distribution of scale-free. This is also proved by Parnell et al. (2009).

Using the definition introduced in Figure 6, we study the orientation angles (θ) of the BMRs. We find that most of the BMRs display a slightly deviated to the solar equator direction on the solar disk, whatever in the northern or southern hemispheres, their median value are 13° and 11° , respectively. The orientation angles of these BMRs are followed by “Hale’s Polarity Laws”, and the polarity of the BMRs is reversed in different solar cycles. We do not find any clearly one by one correlation between the orientation angles and other parameters for all the BMRs. However, if only considering the average values of the orientation angles between -50° and 50° for the normally oriented BMRs during the 23rd solar cycle, the dependence of the orientation angles with latitudes is found as before, which is that the orientation angles increase with the latitudes (see. Figure 11). But for all the BMRs, these with less absolute orientation angles tend to show smaller deviation (e.g., Hale et al., 1919; Wang & Sheeley, 1989; Howard, 1989, 1991a,b).

In this paper, the BMRs in active regions are defined by the closest magnetic poles with opposite polarities, which could result into some wrongly or missing BMRs. Therefore, the errors estimation will be given through comparing the NOAA ARs and our BMRs. Here, the NOAA catalog is assumed to provide the ‘ground truth’. Fig. 12 gives the MDI synoptic charts for CR 1960. In this rotation, 24 BMRs are identified by our method, which are marked with the red pluses (‘+’). At the same time intervals and meridian regions, 30 NOAA ARs are published, as indicated by the turquoise crosses (‘×’). For these identified BMRs, 70% (21/30) of them could be found a one-to-one correspondence with the NOAA ARs, as shown with the overlapping symbols. For these BMRs without the corresponding NOAA ARs, only one (‘I’) maybe not the real BMR because it has the same positive pole with other BMR. The other two (‘II’ and ‘III’) could be the real BMRs as they have the larger and stronger magnetic field with opposite polarities. Therefore, the true identified BMRs from the NOAA ARs could be more than 70%. On the other hand, there are 9 NOAA ARs have missed from our method. Most of these missing NOAA

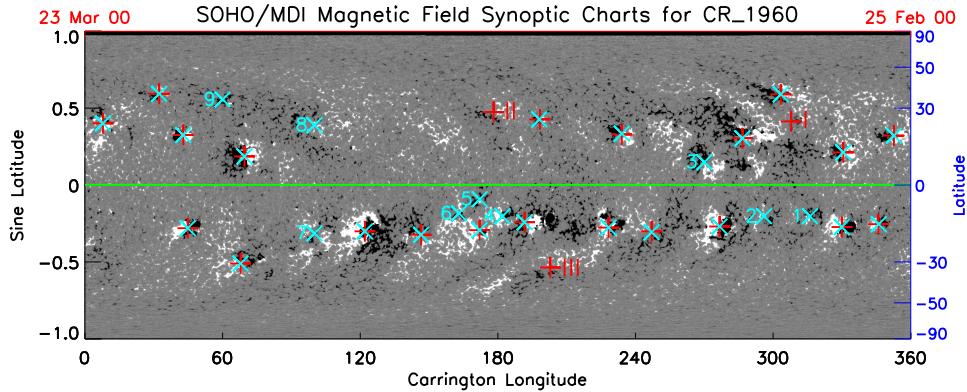


Fig. 12 The synoptic charts from SOHO/MDI magnetograms for CR 1960. The red pluses ('+') mark the positions of the identified BMRs, and the turquoise crosses ('x') indicate the sites of the NOAA ARs.

ARs are possibly not the real BMRs according to our method. Because some of these missing NOAA ARs only display one stronger poles, such as ARs '5', '6' and '9'. Some others have two opposite but very disperse magnetic poles, i.e., ARs '1', '2', '7', and '8'. In a word, our method is useful for these BMRs connecting to the opposite magnetic poles with stronger and compact magnetic fields.

Basing on the computational algorithm, we have automatically identified 2234 BMRs in the active regions from MDI synoptic magnetograms during 1996 to 2010. Meantime, there are total 3171 NOAA ARs published during the same intervals. We could pick up $\sim 70.5\%$ (2234/3171) of the total NOAA ARs. Considering that only these LOS magnetic fields observed near central meridian are used in this paper, some NOAA ARs maybe not appear at the central meridian regions. That is to say, not all the 3171 NOAA ARs could be detected by our observations. Therefore, we can find more than $\sim 70.5\%$ of the appearing NOAA ARs. On the other hand, Fig. 7 (b) shows that the peak distribution of 180 degree is still existent but less obvious than that in panel (a). This peak possible duo to the wrongly identifying BMRs from our computational algorithm. Fig. 8 suggests that these abnormal orientations appear mainly in solar maximum. Based on these facts, we could pick up the wrongly identifying BMRs in solar maximum. At last, 52 (or 77) BMRs are wrongly identified in northern (or southern) hemisphere. And then the accuracy rate is about 94.3%.

Acknowledgements The authors would like to thank the anonymous referee for his/her valuable comments to improve the manuscript. We are indebted to the SOHO/MDI teams and MDI Magnetic Field and Intensity Synoptic Charts for providing the data. This work is supported by NSF of China under Grants 11603077, 11573072, 11333009, the Youth Fund of Jiangsu No. BK20161095, and the Laboratory No. 2010DP173032.

References

- Abramenko, V. I., & Longcope, D. W. 2005, ApJ, 619, 1160
- Aschwanden, M. J., Dennis, B. R., & Benz, A. O. 1998, ApJ, 497, 972
- Aschwanden, M. J., & Parnell, C. E. 2002, ApJ, 572, 1048
- Babcock, H. W. 1961, ApJ, 133, 572
- Berger, T. E., & Lites, B. W. 2003, Sol. Phys., 213, 213
- Bogdan, T. J., Gilman, P. A., Lerche, I., & Howard, R. 1988, ApJ, 327, 451
- Brunner, W. 1930, Astronomische Mitteilungen der Eidgenössischen Sternwarte Zurich, 13, 67

- Canfield, R. C., & Russell, A. J. B. 2007, *ApJ*, 662, L39
- Clauset, A., Shalizi, C. R., & Newman, M. E. J. 2009, *SIAM Review*, 51, 661
- Colak, T., & Qahwaji, R. 2008, *Sol. Phys.*, 248, 277
- Crosby, N. B., Aschwanden, M. J., & Dennis, B. R. 1993, *Sol. Phys.*, 143, 275
- Crosby, N., Vilmer, N., Lund, N., & Sunyaev, R. 1998, *A&A*, 334, 299
- Dennis, B. R. 1985, *Sol. Phys.*, 100, 465
- Domingo, V., Fleck, B., & Poland, A. I. 1995, *Sol. Phys.*, 162, 1
- Hale, G. E., Ellerman, F., Nicholson, S. B., & Joy, A. H. 1919, *ApJ*, 49, 153
- Hathaway, D. H., Wilson, R. M., & Reichmann, E. J. 1999, *J. Geophys. Res.*, 104, 22375
- Hathaway, D. H., Nandy, D., Wilson, R. M., & Reichmann, E. J. 2003, *ApJ*, 589, 665
- Hathaway, D. H. 2010, *Living Reviews in Solar Physics*, 7, 1
- Harvey, K. L., & Zwaan, C. 1993, *Sol. Phys.*, 148, 85
- Howard, R. F. 1989, *Sol. Phys.*, 123, 271
- Howard, R. F. 1991a, *Sol. Phys.*, 132, 49
- Howard, R. F. 1991b, *Sol. Phys.*, 136, 251
- Jiang, J., Cameron, R. H., Schmitt, D., & Schüssler, M. 2011, *A&A*, 528, A82
- Leighton, R. B. 1964, *ApJ*, 140, 1547
- Leighton, R. B. 1969, *ApJ*, 156, 1
- Li, K. J., Yun, H. S., & Gu, X. M. 2001, *AJ*, 122, 2115
- Li, J., & Ulrich, R. K. 2012, *ApJ*, 758, 115
- Li, Y. P., Gan, W. Q., & Feng, L. 2012, *ApJ*, 747, 133
- Li, D., Ning, Z. J., & Wang, J. F. 2013, *New Astronomy*, 23, 19
- Maunder, E. W. 1904, *MNRAS*, 64, 747
- Maunder, E. W. 1922, *MNRAS*, 82, 534
- McAteer, R. T. J., Gallagher, P. T., & Ireland, J. 2005, *ApJ*, 631, 628
- McKinnon, J. A., & Waldmeier, M. 1987, "Sunspot numbers, 1610-1985 : based on "The sunspot activity in the years 1610-1960" , by McKinnon, John A.; Waldmeier, Max. Boulder, Colo. : World Data Center A for Solar-Terrestrial Physics, [1987]. Report UAG, 0579-7144 ; 95. . World Data Center A for Solar-Terrestrial Physics.
- Ning, Z., Wu, H., Xu, F., & Meng, X. 2007, *Sol. Phys.*, 242, 101
- Parnell, C. E., DeForest, C. E., Hagenaar, H. J., et al. 2009, *ApJ*, 698, 75
- Scherrer, P. H., Bogart, R. S., Bush, R. I., et al. 1995, *Sol. Phys.*, 162, 129
- Schrijver, C. J. 1988, *A&A*, 189, 163
- Schrijver, C. J., Title, A. M., van Ballegoijen, A. A., Hagenaar, H. J., & Shine, R. A. 1997, *ApJ*, 487, 424
- Sheeley, N. R., Jr., DeVore, C. R., & Boris, J. P. 1985, *Sol. Phys.*, 98, 219
- Shetye, J., Tripathi, D., & Dikpati, M. 2015, *ApJ*, 799, 220
- Song, Q., Huang, G., & Tan, B. 2012, *ApJ*, 750, 160
- Su, Y., Gan, W. Q., & Li, Y. P. 2006, *Sol. Phys.*, 238, 61
- Tang, F., Howard, R., & Adkins, J. M. 1984, *Sol. Phys.*, 91, 75
- Temmer, M., Veronig, A., & Hanslmeier, A. 2002, *A&A*, 390, 707
- Tran, T., Bertello, L., Ulrich, R. K., & Evans, S. 2005, *ApJS*, 156, 295
- Ulrich, R. K., Bertello, L., Boyden, J. E., & Webster, L. 2009, *Sol. Phys.*, 255, 53
- Wang, Y.-M., & Sheeley, N. R., Jr. 1989, *Sol. Phys.*, 124, 81
- Wheatland, M. S. 2000, *ApJ*, 536, L109
- Wheatland, M. S. 2003, *Sol. Phys.*, 214, 361
- Wolf, R. 1861, *MNRAS*, 21, 77
- Zhang, J., Wang, Y., & Liu, Y. 2010, *ApJ*, 723, 1006
- Zharkov, S., Zharkova, V. V., & Ipson, S. S. 2005, *Sol. Phys.*, 228, 377
- Zharkov, S. I., & Zharkova, V. V. 2006, *Advances in Space Research*, 38, 868